Journal of Electroceramics 1:2, 179–192, 1997

Study of Ion Distribution in Nd(III) Doped β''-Alumina through Atomistic Simulation

YUHU WANG & ALASTAIR N. CORMACK
New York State College of Ceramics, Alfred University Alfred, NY 14802

Submitted January 28, 1997; Revised April 22, 1997; Accepted April 30, 1997

Abstract. β''-aluminas doped with Nd^{3+}, in both stoichiometric ($Na_2MgAl_{10}O_{17}$) and non-stoichiometric ($Na_{1.66}Mg_{0.66}Al_{10.33}O_{17}$) forms, have been studied through atomistic computer simulation. The optimum distribution of Mg^{2+} in the spinel blocks, Na^+ as well as Nd^{3+} in the conduction planes have been calculated and discussed in comparison with the structure models derived experimentally. Mg^{3+} ions prefer to occupy the tetrahedral Al(2) sites in the spinel blocks, and show strong tendency to form two- or three-membered clusters. Due to the presence of Mg^{2+}, oxygen ions in or adjacent to the conduction plane, O(5), O(4) and O(3), are displaced from their ideal sites, leading to the removal of the local symmetry at the mO site in parent β''-alumina. Doped Nd^{3+} ions are calculated to be preferentially located in the vicinity of the mO sites (9d) and their displacement from the ideal mO site is strongly affected by the distribution of Mg^{2+} and nearby Na^+ vacancy. The bridging oxygen in the conduction plane, O(5), relaxes off its original position towards the Nd^{3+} ions by $\sim$0.39Å, which is in excellent agreement with previous X-ray diffraction and EXAFS studies. The oxygen ions in the spinel block, O(3) and (4), are attracted towards Nd^{3+} non-uniformly, whereas the nearest Al(6c) ions are displaced in the opposite direction. The picture for the local structure clearly shows that the inversion symmetry at the Nd^{3+} position is absent, due to the non-uniform displacement of surrounding oxygen atoms from their ideal positions.

Keywords: β''-alumina, atomistic simulation, Nd^{3+}, distribution, conduction plane

1. Introduction

β''-alumina doped with optically active ions has attracted much attention in recent years, due to its excellent optical properties and potential application as a new solid state laser medium. It has been found that rare earth doped β''-alumina shows anomalously strong optical absorption, e.g., Nd(III) β''-alumina showed oscillator strengths for the $^4I_{9/2} \rightarrow {}^4G_{5/2}, {}^2G_{7/2}$ transition 10 times as high as that of Nd(III) YAG. In 1984, the first laser action was achieved [1] and subsequently optical phase conjugation [2] and degenerate four wave mixing (DFWM) have been demonstrated in Nd(III) doped β''-alumina.

In order to develop it as a new, high output power laser host, a thorough understanding of the fluorescence process of the doped ions, such as Nd^{3+}, in β''-aluminas is necessary, which in turn requires detailed knowledge of the local structure of Nd^{3+} ions. During the past decade, much effort has been exerted in clarifying the ionic distribution in β''-aluminas, including those doped with various rare earth cations, through a variety of approaches. Stoichiometric β''-alumina has a chemical composition of $Na_2MgAl_{10}O_{17}$ but, normally, it appears in a non-stoichiometric form, typically with a composition of $Na_{1.66}Mg_{0.66}Al_{10.33}O_{17}$. The structure of β''-alumina has rhombohedral symmetry, in space group $R\bar{3}m$. There are three spinel-like blocks, which are sandwiched by three ''conduction planes'', in a unit cell. The blocks consist of close packed oxygen layers with Al, Mg atoms, and are referred to as ''spinel blocks'' because of the structural resemblance to the mineral spinel $MgAl_2O_4$, (Fig. 1). The spinel blocks are connected through a bridging oxygen, O(5), in the conduction plane. Around the O(5), Na^+ ionic migration can occur through two-dimensional honeycomb-like pathways, due to the ''open'' structure of

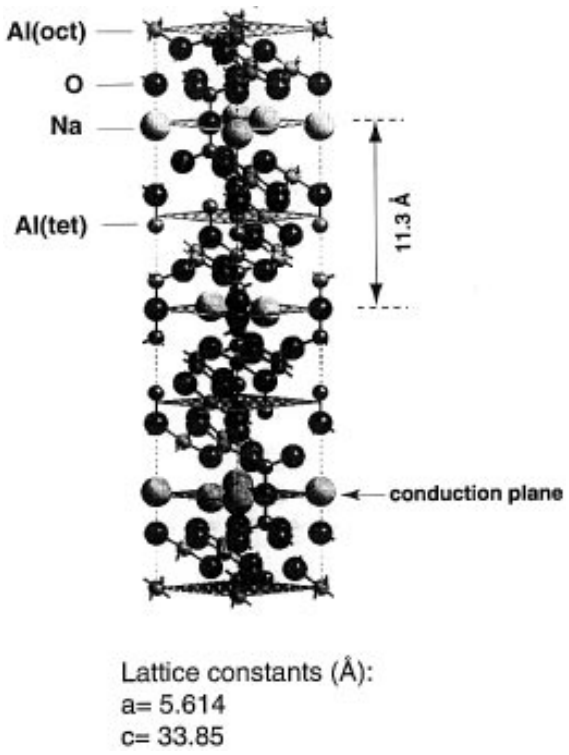

Fig. 1. Crystal structure of ideal β''-alumina.

the plane. This ''open'', disordered area is about 3.9 Å thick [3] and makes it possible to dope large amounts of active rare earth ions through low temperature (<650°C) ion exchange techniques [4]. Because of this disorder feature, however, conventional diffraction techniques encounter serious intrinsic difficulties in providing detailed information about the structure of the conduction planes.

When exchanged for Na^+, Nd^{3+} can occupy non-equivalent sites in the conduction plane: the seven-coordinated Beevers-Ross type site (BR), the eight-coordinated mid-oxygen sites (mO), or 18 h site which is midway between the BR and mO sites. In spite of extensive studies, the site which Nd^{3+}, or other similar cations, prefer to occupy remains controversial, although it is well known that rare earth ions in oxides have a strong tendency to occupy high coordination sites. Davies et al. suggested [5], on the basis of high resolution TEM observation, that 60% of Nd^{3+} is located in the BR sites with the remaining 40% in the mO sites. Subsequently, from single crystal X-ray diffraction studies [6], Carrillo-Cabrera et al. argued that lanthanide ions strongly prefer the mid-oxygen site. Their study also showed significant displacement of the bridging oxygen, O(5), toward the mO site. Bush et al. [7] performed both static-lattice defect-energy calculations and MD simulations on Nd^{3+} doped β''-alumina and obtained results suggesting that Nd^{3+} resides preferentially midway between the BR and mO sites, in 18 h positions, which is inconsistent with the X-ray diffraction study. Also through single crystal diffraction, Wolf et al. [8] recently showed that Nd^{3+} was distributed in a ratio of 60 : 40 between the mO and BR sites in the 60% exchanged β''-alumina and 95 : 5 in the 100% exchanged sample, which was supported by their MD simulations [9]. More recent XANES, EXAFS study by Rocca et al . [10] supported the earlier X-ray diffraction studies that most Nd^{3+} reside in the mO sites. They also saw indications for the displacement of those ions surrounding Nd^{3+}.

As shown in Fig. 2a, the ideal mO site has C_{2h} point group symmetry and is thus a center of inversion symmetry. Consequently, if the rare earth ions sit on mO site, electric-dipole transitions are forbidden and no strong absorption should be observed in the optical spectra, unless the symmetry is broken by local environment changes. On the other hand, the BR site has C_{3v} symmetry and an electric-dipole transition is

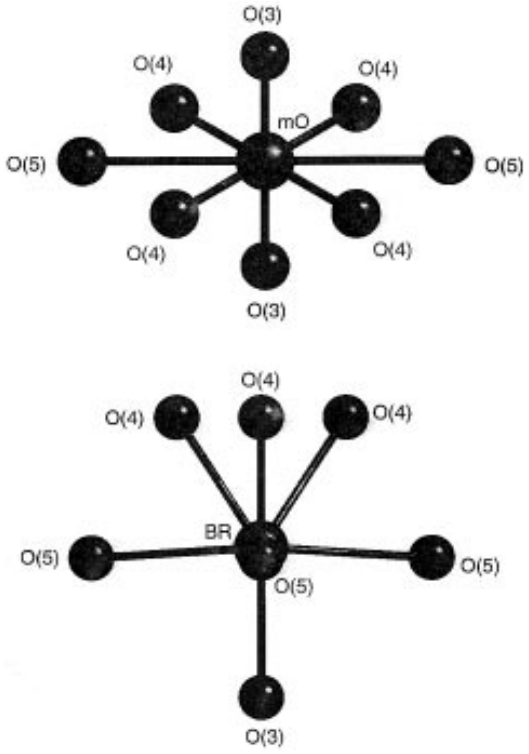

Fig. 2. Nd^{3+} in (a) ideal Beevers-Ross site and (b) mid-oxygen site.

allowed, since there is no inversion symmetry (Fig. 2b). Whilst most X-ray diffraction studies claimed that Nd reside in the mO site, strong absorption, which is dependent on the dopant concentration, has been observed with Nd doped β''-aluminas. To explain the optical properties in terms of the local structure of Nd^{3+} and be consistent with the X-ray study, Alfrey et al. proposed a structure model [11] in which the bridging oxygen O(5) and the Nd^{3+} relaxed slightly off their original sites and thus the inversion symmetry was broken. They claimed that the shift is induced by the non-uniform distribution of Na^+ ions. However, it is difficult to demonstrate such a local structural change using conventional diffraction techniques, which only provide time and space averaged information. The model by Alfrey et al. has not yet been confirmed experimentally.

In this study, we examined the structure of Nd(III) β''-alumina through detailed static lattice energy calculations, with a focus on the ionic distribution and the local environment change upon the substitution of Na^+ with Nd^{3+}. Our objective is to provide a local structure model, which might be used to explain the optical properties of Nd(III) β''-alumina. This work is a part of our systematic studies on the structure of hexa-aluminate system through computer modeling [12].

2. Simulation Methods

Our calculations are based on the Born model, which treats the solid as a collection of point ions with short-range forces acting between them. The simulation methods in this study are exactly the same as in our previous studies [12–14]. The approach has enjoyed a wide range of success. The potential parameters were taken from the compilation of Lewis and Catlow [15] and are listed in Table 1. The O–O parameters were taken from the works of Catlow [16]. Since they can be found in those references [12–14] and thereafter, the theoretical basis behind our simulation and the details of the procedures will not be discussed here.

Calculations were performed on either the Silicon Graphics Workstations in our laboratory or the IBM SP2 Parallel Supercomputer at the Cornell Theory Center, Cornell University, depending on the lattice structure input models chosen.

Table 1. Interatomic potential parameters used in calculations

a) Short-range parameters for potential form $V(r) = A\exp(-r\rho^{-1}) - Cr^{-6}$

Interaction	A(eV)	ρ(Å)	C(eV Å^{-6})
Na-O	611.08	0.35350	0.000
Mg-O	821.60[710.50]	0.3242	0.000
Al-O	1474.40[1334.31]	0.30059	0.000
Nd-O	1379.90	0.36010	0.000
O-O	22764.20	0.14910	17.890

* Values of A in brackets are for cations in a tetrahedral center.

b) Shell model parameters

Interaction	Shell charge Y(e)	Spring constant k(eV Å^{-2})
Na(core)-Na(shell)	1.000	∞
Mg(core)-Mg(shell)	2.000	∞
Nd(core)-Nd(shell)	3.000	∞
Al(core)-Al(shell)	3.000	∞
O(core)-O(shell)	−2.207	27.27

3. Results and Discussion

3.1. Mg^{2+} Distribution in the Spinel Block

Bettman and Peters [17] were the first to identify the structure of β''-aluminas stabilized by Mg^{2+}, through X-ray diffraction on a single crystal. Using their X-ray derived coordinates as our input model (Table 2), we were able to establish an equilibrium perfect lattice structure. We first performed our simulation on both the undoped stoichiometric β''-aluminas, $Na_2MgAl_{10}O_{17}$ and non-stoichiometric β''-aluminas, $Na_{1.66}Mg_{0.66}Al_{10.33}O_{17}$. In the stoichiometric structure, since all the BR-type sites are occupied by the six Na^+ ions in a unit cell, we can concentrate on the question how the three Mg^{2+} ions are distributed in the three spinel blocks as charge compensators or stabilizers, which turned out to be a crucial factor affecting the distribution of other ions.

There are altogether four non-equivalent Al sites (Table 2), either octahedral or tetrahedral, that Mg^{2+} may occupy. Since their scattering factors are very close, it is difficult to distinguish between Al and Mg with X-ray diffraction. Bettman and Peters, on the basis of electrostatic considerations, decided that the Mg^{2+} would be found in the vicinity of the conduction plane to compensate for the excess charge of the conduction plane [17]. Later, such a Mg distribution

Table 2. Structural parameters for β''-alumina ($Na_{1.66}Mg_{0.66}Al_{10.33}O_{17}$), Ref. 17

lattice constants (Å)			**a** = 5.614
Atom	Wyckoff notation	Type of site	**c** = 33.85
O(1)	18 h	tetrahedral	x 0.1562
			z 0.0339
O(2)	18 h	tetrahedral	x 0.1657
			z 0.2357
O(3)	6c	tetrahedral	x 0
			z 0.2955
O(4)	6c	tetrahedral	x 0
			z 0.0961
O(5)	3b	linear	x 0
			z 1/2
Al(1)	18 h	octahedral	x 0.3362
			z 0.0708
Al(2)	6c	tetrahedral	x 0
			z 0.3501
Al(3)	6c	tetrahedral	x 0
			z 0.4498
Al(4)	3a	octahedral	x 0
			z 0
Na	6c	BR	x 0
			z 0.1719

in β''-aluminas was found to be incorrect by neutron diffraction study, which is more powerful in distingushing between Mg and Al, due to their different neutron scattering factors. The neutron diffraction studies demonstrated that β''-aluminas are stabilized with the tetrahedral Al(2) site partially (∼37%) substituted by Mg^{2+} in the center of the spinel blocks [18–20]. Because the mean Al(Mg)...O distance at Al(2) is longer than in β-aluminas where Mg also resides in the tetrahedral Al site as impurity, Thomas et al. suggested that Mg^{2+} plays a role as a strain reliever in β''-aluminas [19]. Further neutron diffraction study on samples with different heat treatments, by Alden et al., suggested that the degree of long-range ordering of adjacent Mg/Al(2) is affected by the quenching rate [21]. Recently, Hafskjold and Li demonstrated [22], based on MD simulations on Na β''-aluminas, that the vacancy superlattice in the conduction plane depends crucially on the Mg^{2+} distribution. They also showed that electrical conductivity or diffusion coefficient is strongly influenced by the Mg^{2+} distribution [22].

Our calculations give the same results as the neutron diffraction study that the Mg^{2+} ions prefer to reside evenly in the tetrahedral Al(2) sites, since such a configuration leads to the lowest lattice energy. Although there are many configurations for the three Mg^{2+} distributed over 33 possible Al sites in a unit cell, our calculations demonstrate that Mg^{2+} ions tend to disperse as evenly as possible in the tetrahedral Al(2) sites in reaching the most stable state. Any non-uniform distribution of Mg will give rise to increase in the lattice energy of about 1–4 eV. For example, for the three Mg^{2+} distributed in the six Al(2) sites, there are four unequivalent configurations with corresponding lattice energies being −2595.39 eV, −2595.91 eV, −2598.90 eV and −2598.98 eV. The most even distribution has the lowest value −2598.98 eV. Table 3 gives the calculated lattice energies for the stoichiometric lattice unit with three Mg evenly distributed in different Al sites.

How Mg^{2+} is distributed in the Al(2) site is an crucial issure. For reasons which will become clear, we established a $\sqrt{3}\mathbf{a} \times \sqrt{3}\mathbf{b} \times \mathbf{c}$ triple superlattice structure for further calculation. There are nine Mg^{2+} to be distributed in eighteen Al(2) sites and thus numerous configurations of Mg distribution become possible in the triple cell. Following the calculation results on the single cell, even distributions for the nine Mg^{2+} in the three spinel blocks, *i.e.*, with each spinel block accomodating three Mg^{2+}, lead to lower lattice energies than other non-uniform distributions. Under such a condition, the large number of possible configurations has been greatly reduced, and we are able to calculate the lattice energies of the limited, possible configurations for Mg^{2+} in Al(2) in the supercell. In each spinel block, the three Mg^{2+} can either evenly disperse or partially or completely agglomerate. In Figs. 3 and 4 are shown two representative configurations, with their lattice energy listed in Table 3. One has the lowest lattice energy among all the possible configurations (Fig. 4) and the other is for the most even distribution of Mg^{3+} in Al(2) sites (Fig. 3).

In the following discussion, we will refer to the

Table 3. Calculated perfect lattice energies for distribution of three Mg^{2+} ions in Al sites in stoichiometric β''-alumina ($Na_2MgAl_{10}O_{17}$)

Site	type of site	lattice energy (eV)	Supercell *E*/3
Mg^{2+} at Al(1)1,7,13	octahedral	−2596.47	
Mg^{2+} at A1(2)2,4,6	tetrahedral	**−2598.98**	
Mg^{2+} at Al(3)2,4,6	tetrahedral	−2594.13	
Mg^{2+} at Al(4)	octahedral	−2597.67	
Model I (triple cell)	tetrahedral	−7796.94	**−2598.98**
Model II (triple cell)	tetrahedral	−7798.59	**−2599.53**

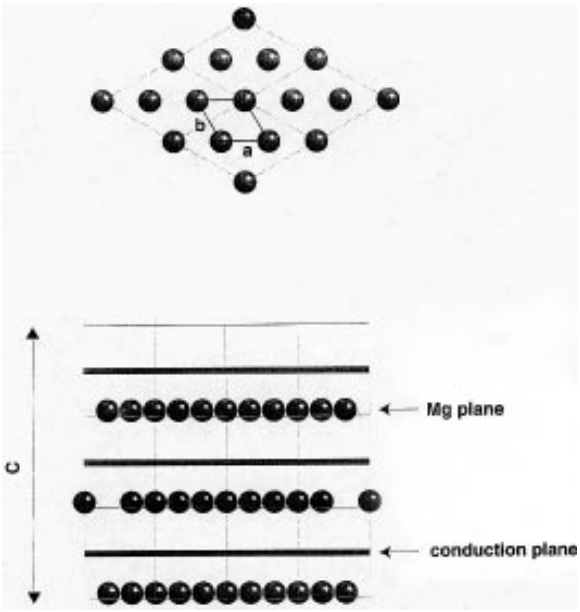

Fig. 3. Mg distribution in the Model I structure for stoichiometric β''-alumina. (a) planar view of a Mg plane, with a basic single unit cell being shown. (b) view from [110] direction.

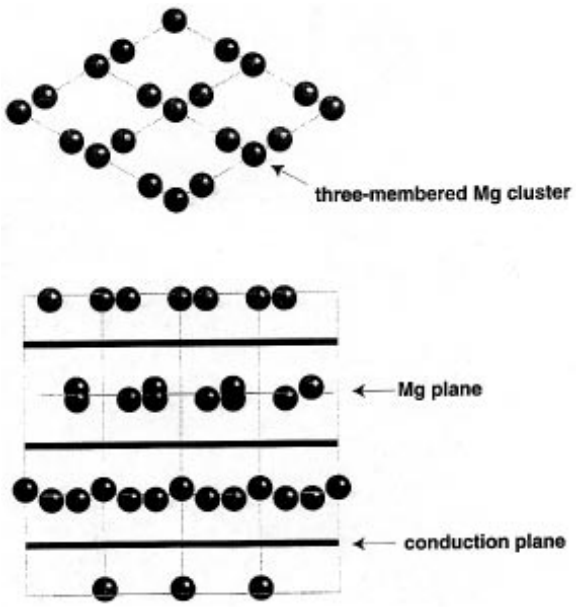

Fig. 4. Mg distribution in the Model II structure for stoichiometric β''-alumina. (a) planar view of a Mg plane, (b) view from [110] direction.

configurations of Fig. 3 and 4 as Model I and II, respectively. The configuration for Model I is possible, even with a basic unit cell where the three Mg^{2+} ions occupy either the Al(2) 2, 4, 6 or equivalently, Al(2) 1, 3, 5 positions. In such a configuration, all the Mg^{2+} are separated by equal distance on the same plane (Fig. 3a). While there is no difference between the basic unit cell and the triple supercell for Model I, Model II configuration is only available with a triple superlattice unit cell. Similarly to Model I, three Mg ions are introduced into each spinel block, but they occupy the Al(2)1, 2, 3, 4, 5, 6 positions instead. In the same plane, Mg ions are no longer separated by equal distances, rather they form a three-membered cluster (Fig. 4a). Note that E/3 for the triple cell of Model II is lower than E of the corresponding single unit cell by $\sim$0.6 eV. The calculated lattice energy shown in Table 3 suggests that Model II is more stable than Model I. Therefore, we can conclude that Mg^{2+} ions, as stabilizers, prefer to occupy the tetrahedral Al(2) site and tend to aggregate to form the three-membered cluster in stoichiometric β''-aluminas.

For the non-stoichiometric β''-aluminas, we need to remove one Na and replace one Mg with an Al in the stoichiometric single unit cell. It becomes not possible to allow the two Mg^{2+} ions to be evenly distributed into the three spinel blocks in a single unit cell. A $\sqrt{3}\mathbf{a} \times \sqrt{3}\mathbf{b} \times \mathbf{c}$ triple superlattice (derived either from Model I or from Model II) is necessary for uniform distribution. The most preferred, energetically stable, configuration turned out to be that which takes one Na from each conduction plane and one Mg from each Mg plane in the triple superlattice, for both Models I and II, with Mg^{2+} still sitting at the Al(2) site (Figs. 5 and 6). The three-membered Mg cluster now becomes a two-membered cluster in Model II (Fig. 6a). E/3 for both Models are lower than the lowest lattice energy E calculated with a single unit cell, where two Mg ions are located in the Al(2) sites in the

Table 4. Calculated lattice energies for non-stoichiometric β''-alumina ($Na_{1.66}Mg_{0.66}Al_{10.33}O_{17}$) with Mg^{2+} ions at Al(2)

Model	type of site	lattice energy (eV)	$E/3$
single cell	Al(2)2,4	−2622.09	
Model I (triple cell)	Al(2)2,4,6	−7870.50	**−2623.50**
Model II (triple cell)	Al(2)1,2,3,4,5,6	−7871.47	**−2623.82**

Table 5. Calculated defect energies for the stoichiometric ($Na_2MgAl_{10}O_{17}$) and non-stoichiometric β''-alumina ($Na_{1.66}Mg_{0.66}Al_{10.33}O_{17}$)

	Defect energy (eV)			
	$Na_2MgAl_{10}O_{17}$		$Na_{1.66}Mg_{0.66}Al_{10.33}O_{17}$	
energy type	Model I	Model II	Model I	Model II
E_1	4.424, 4.485	4.447, 4.468	5.172, 5.144	5.176, 5.169
E_2	−29.72, −29.92	−29.78, −29.87	−30.09, −30.56	−30.33, −30.59
E_3	−26.35	−26.29	−25.68	−25.64
$E_a(1)$*	−0.854	−0.867	−0.264	−0.219
E_4	−21.95	−21.77	−20.73	−20.69
$E_a(2)$*	−0.878	−0.794	−0.458	−0.438

*$E_a(n)$ is the association energy, which is defined as:

$$E_a(1) = E_3 - E_1 - E_2$$

$$E_a(2) = E_4 - 2E_1 - E_2$$

where the lower E_1 and E_2 values are used.

spinel blocks with one of the conduction planes being Na vacant. This result comes from the effect of a more even distribution of Na vacancy and Mg in the triple cell than in the single unit cell. Again, Model II is more stable than Model I, in terms of the lower lattice energy (Table 4).

For the nonstoichiometric β''-alumina, the presence of Na vacancy (V'_{Na}, one per unit cell or $0.33\,V'_{Na}$ in

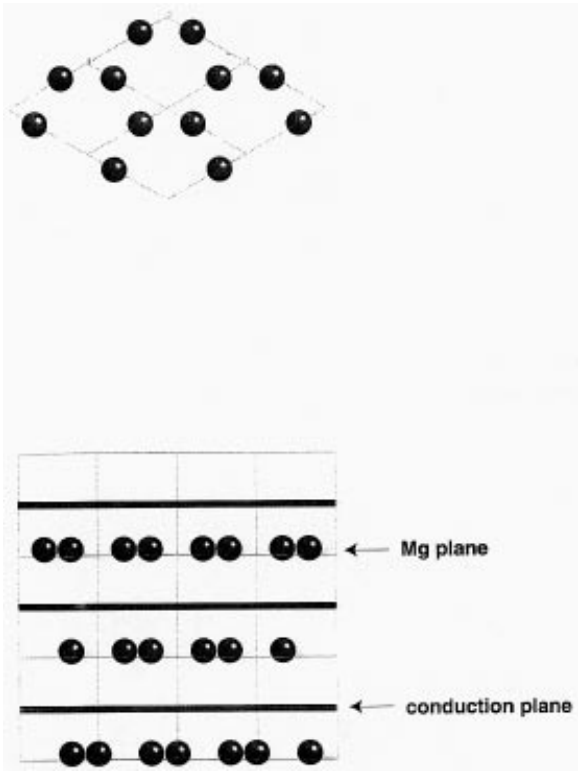

Fig. 5. Mg distribution in the Model I strucuture for non-stoichiometric β''-alumina. (a) planar view of a Mg plane, (b) view from [110] direction.

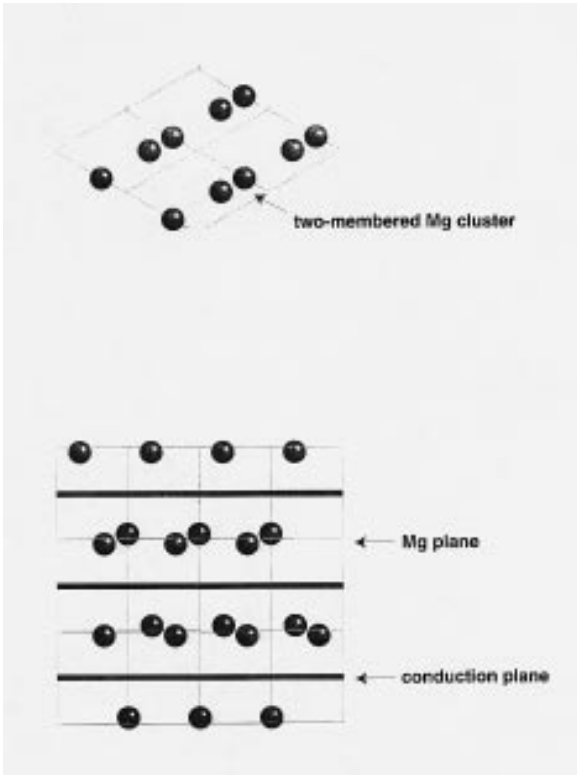

Fig. 6. Mg distribution in the Model II structure for non-stoichiometric β''-alumina. (a) planar view, (b) iew from [110] direction.

each conduction plane), needs to be taken into account. With the triple cell, we can create one V'_{Na} in each conduction plane to let the V'_{Na} disperse evenly. Figure 7 shows the conduction planes for both the stoichiometric and the nonstoichiometric structure. In the latter, the three Na^+ ions surrounding the V'_{Na} tend to relax off their original BR sites towards the V'_{Na} in the nonstoichiometric conduction plane (Fig. 7b), in either Model I or II, although to a slightly different degree. As a result, the originally equivalent Na ions are distributed into two non-equivalent positions: BR sites, and 18 h sites, the site which is adjacent to the Na vacancy. This is in agreement with other studies. Using diffuse X-ray scattering, Boilot et al. have already observed that Na^+ ions in β''-alumina are localized on independent BR sites and the 18 h position [23]. The Na vacancies are ordered to form a 2D triple supercell, which is the same as Fig. 7b. Wolf et al., through MD simulation, calculated the relaxation of Na^+ towards V'_{Na} as 0.81 Å [24]. The similar relaxation of Na^+ in our model turned out to be 0.73–0.79 Å for Model II, not exactly uniform though, and is close to Wolf et al.'s calculation.

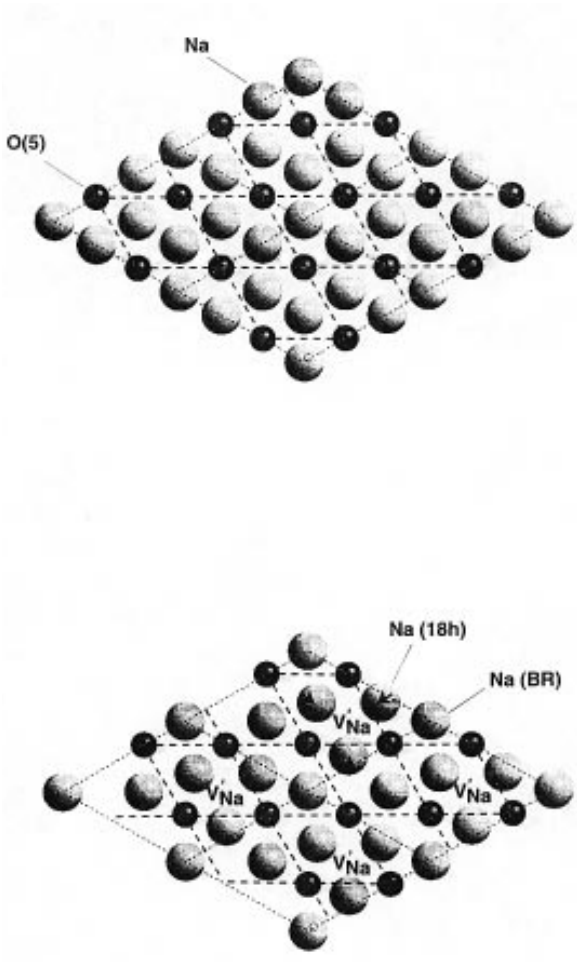

Fig. 7. Conduction plane of (a) stoichiometric (b) non-stoichiometric β''-alumina. V_{Na} forms a 2D triple superlattice.

3.2. Nd^{2+} Preferred Site

3.2.1. Stoichiometric β''-Alumina. With the optimized structure for either the stoichiometric and nonstoichiometric parent β''-aluminas, we were then able to calculate the sites of Nd^{3+} which is exchanged for Na^+ in the conduction plane, and the structural changes occurring locally around the Nd^{3+}. In the following discussion, we will be focused on the Model II structure due to its higher stability, but the results on Model I will also be presented for comparison. Basically, to introduce one Nd^{3+}, one needs to remove three Na^+ for charge neutrality. But for a more complete analysis, the following substitution processes which include defect interactions are considered:

$$Na_{plane} \rightarrow V'_{Na} + Na^+ \quad (1)$$

$$Nd^{3+} + Na_{plane} \rightarrow Nd_{plane} + Na^+ + V'_{Na} \quad (2)$$

$$Nd^{3+} + 2Na_{plane} \rightarrow Nd_{plane} + 2Na^+ + 2V'_{Na} \quad (3)$$

$$Nd^{3+} + 3Na_{plane} \rightarrow Nd_{plane} + 3Na^+ + 3V'_{Na} \quad (4)$$

where Na_{plane} and Nd_{plane} denote the Na^+ and Nd^{3+} ions in the conduction plane, respectively; V'_{Na} the Na^+ vacancy; Nd^{3+} is to be introduced into the system for substitution; Na^+ the replaced ion that is taken out of the system.

In process (1), a Na^+ vacancy (V'_{Na}) is formed, whilst in other processes (2), (3) or (4), one or more Na^+ ions are substituted by one Nd^{3+}. Note that these defects, except that caused by process (4), are not electrostatically neutral; there is no requirement for this as long as other V'_{Na} are simultaneously created, to keep the crystal on a whole charge balanced. The more the V'_{Na} are created, the more the possible configurations for V'_{Na}. The defect energies for substitution, E_i, summarized in Table 5 are calculated for the typical configurations which will be discussed later. As a measure of defect stabilities, the association energy (with respect to isolated defects), $E_a(n)$, is calculated from the defect energy and also shown in Table 5.

The X-ray derived space group symmetry requires that all the BR sites be equivalent. Our calculation of the Na^+ vacancy energy, E_1 as well as subsititution energy E_2, however, results in two different values, implying that there are two unequivalent BR sites. The difference between the two E_1 values is less significant in Model II compared with Model I (Table 5), indicating that the BR sites in Model II structure are closer to the ''ideal position'' (X-ray derived). Although no experimental data are available to allow comparison, our calculations indicate that the existence of Mg^{2+} as stabilizer actually causes the crystal structure to be distorted, with the oxygen ions shifted off their ideal positions. From a magnified picture of mO sites in the optimized structure (Fig. 8), it can be seen that the X-ray defined mO site in the ideal structure, used as input model, is in a center of symmetry, whereas there is no symmetry in the mO sites in either Model I or II, due to the displacement of oxygen, from their original site. Model I structure has more strain than Model II, in terms of the more significant displacement from its ideal mO positions (Fig. 8b). Such a displacement caused by Mg^{2+} is responsible for the non-equivalent BR positions in the conduction plane. The reason why Model I shows more distortion than Model II can be seen from Figs. 3b and 4b, the view for the Mg distribution from [110] direction. In Model I, though they are evenly distributed on the same plane, Mg ions are off the symmetric position with respect to the spinel block center or the conduction planes. In spite of the cluster configuration, however, the overall Mg distribution in Model II structure is more symmetric and uniform. Therefore, the distribution of electron density, or the influence from Mg upon the conduction plane, should be more uniform in the Model II structure, resulting in less strain and less displacement of the oxygen ions from their ideal positions.

Our calculations showed that the final position for Nd^{3+} depends on (a) the distribution of Mg^{2+} and (b) the configuration of nearby V'_{Na}. In process (2), where one Na^+ is replaced by one Nd^{3+}, the Nd^{3+} stays at the original Na site, the seven-coordinated BR site, because of the highly symmetric configuration. In contrast, in process (3), Nd^{3+} always relaxes off the BR site towards the mO site, which is midway between the two adjacent vacant BR sites, and finally resides in a displaced mO site (Fig. 9). The defect energy E_3 in Table 5 is calculated for the configuration where two adjacent Na, as positioned at 1 and 2 in Fig. 9, are replaced by Nd^{3+}, which is initially located on one of the Na positions. Since E_3 is lower than $(E_1 + E_2)$ by about 1 eV (represented by $E_a(1)$ in

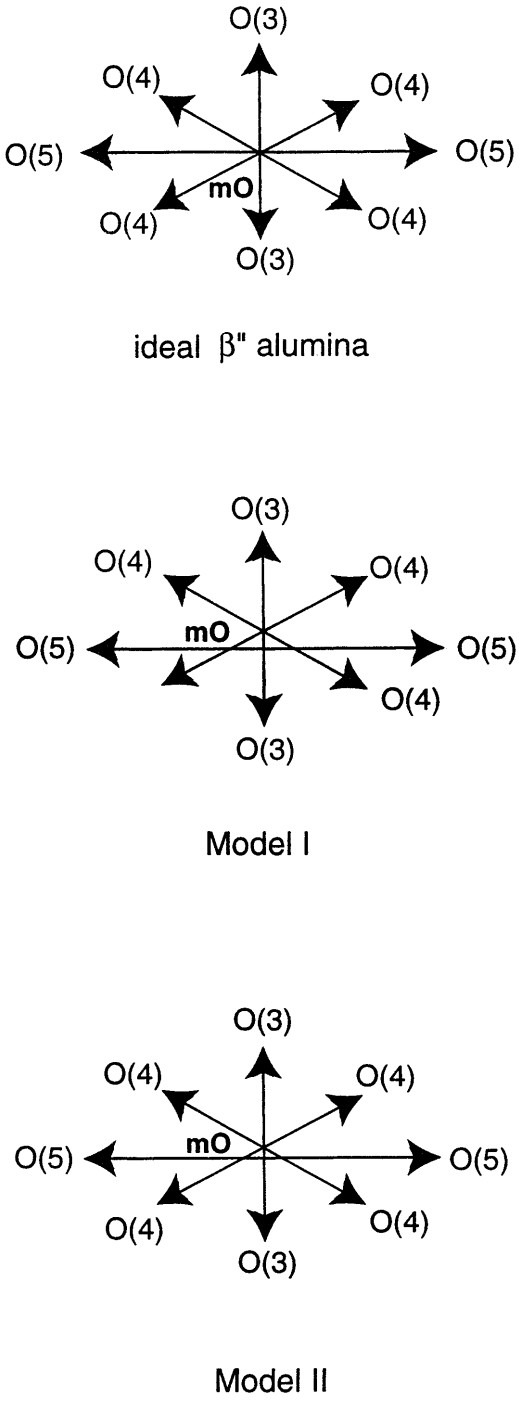

Fig. 8. Magnetified picture of mO site in (a) ideal, (b) Model I, and (c) Model II β''-alumina structures.

Table 5), for either Model I or Model II, the defect structure due to the process (3) is preferred to that of process (2), i.e., the defect $V_{Na}(1)\ldots Nd\ldots V_{Na}(2)$ with one doped Nd^{3+} sitting at displaced mO (see Fig. 9) is more stable than the defects V'_{Na}, Nd_{plane} formed independently. Comparing between Models I and II, the displacement of Nd from the ideal mO site is more significant in Model I structure.

In reality, when one Nd^{3+} is introduced, three Na^+ ions need to be removed to keep the charge balanced, as in process (4). Processes (2) and (3) can be treated as the extreme cases of (4) when some V'_{Na} are created, simultaneously, far away from Nd^{3+}. The simplest configuration for process (4) is to replace three adjacent Na^+ positioned at 1, 2, 3, as depicted in Fig. 9, with one Nd^{3+}. This turned out to be unstable, e.g., in Model II structure, the second-nearest Na vacancy, positioned at 3 in Fig. 9, tends to be occupied by another Na which displaces from position 4. Again, Nd relaxes off its initial BR site towards the mO site. Our calculation showed that the Nd^{3+} still tends to be associated with only two nearest Na^+ vacancies, with the third V'_{Na} (the next nearest) remaining some distance from the Nd^{3+}. This means that the Nd is not in the center of the triple Na^+ vacancy cluster. The E_4 shown in Table 5 for the stoichiometric structure is calculated for the configuration where Na at positions 1, 2, 5 were replaced by Nd. This is among the most stable configurations in our calculations for process (4). Since this E_4 is quite close to $(E_3 + E_1)$ in Table 5, we may predict that the third V_{Na} has little interaction with the associated defect $V'_{Na}(1)\ldots Nd\ldots V'_{Na}(2)$.

The trend of structure relaxation due to process (4) in Model I structure is similar to that in Model II, except for the more significant displacement of Nd from the ideal mO position.

3.2.2. Nonstoichiometric β''-Alumina. The defect process in the non-stoichiometric β''-alumina is somewhat different to those occurring in the stoichiometric β''-alumina, due to the different distribution of Mg and the presence of intrinsic V'_{Na} in the conduction plane, which has an influence on the equilibrium position of Nd. For example, Nd^{3+} substituted for one Na^+ in process (2) also tends to move towards mO: if a Na at the BR site is substituted, Nd will stay midway between the mO and BR sites; whereas if a 18 h Na is substituted, the final equilibrium position for Nd will be a displaced mO site. Because of the lower E_2 value to replace a 18 h

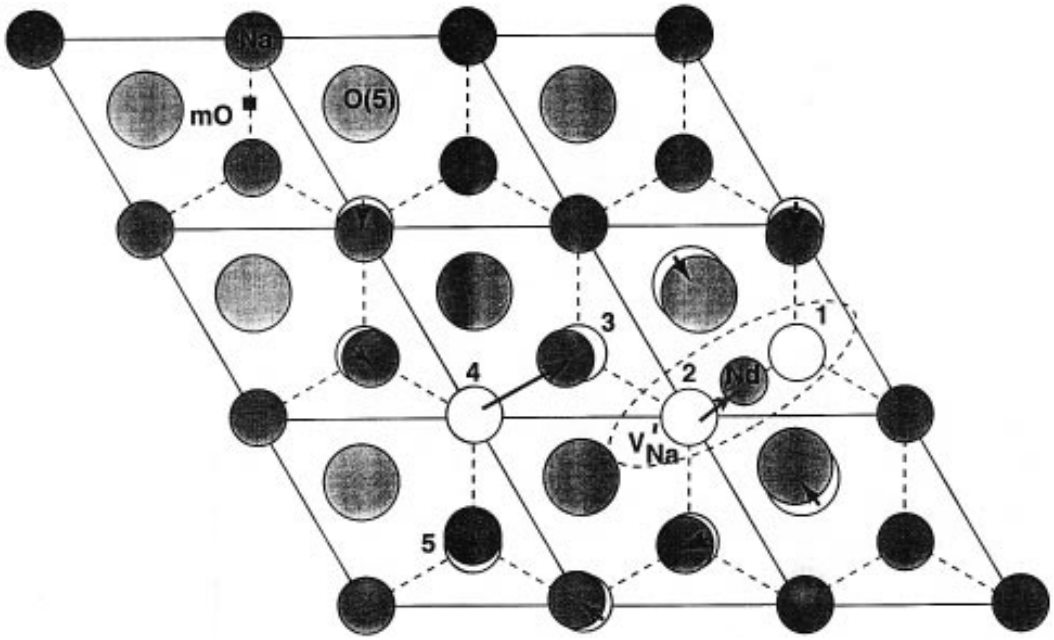

Fig. 9. Structural relaxation upon introduction of one Nd for substitution of three Na^+ positioned at 1, 2, 3 in the stoichiometric conduction plane. The defect $V_{Na}(1)\ldots Nd\ldots V_{Na}(2)$ is shown by the dotted oval.

Na than a BR Na in the process (2), the displaced mO site is thus preferred.

While many defect configurations are possible for processes (3) and (4), a preference for the defect structure where two adjacent V'_{Na} are associated with a Nd^{3+} sitting on a displaced mO site, $V'_{Na}(1)\ldots Nd\ldots V'_{Na}(2)$ is again demonstrated by our calculation on the non-stoichiometric β''-alumina. The next-nearest V'_{Na} tends not to be associated with the $V'_{Na}(1)\ldots Nd\ldots V'_{Na}(2)$ defect, i.e. the Nd is also not in the center of the triple Na^+ vacancy cluster in the non-stoichiometric β''-alumina, as shown in Fig. 10. Those features have already been seen with the stoichiometric β''-alumina. But unlike in the stoichiometric β''-alumina, the V'_{Na} associated with Nd can either be created due to the introduction of Nd^{3+} or be the originally present, intrinsic V.

In Table 5 also are summarized the defect energy E_i for the nonstoichiometric β''-alumina in which the defect $V'_{Na}(1)\ldots Nd\ldots V'_{Na}(2)$ is always involved. Since there are two inequivalent Na sites, BR and 18 h, the two unequal E_1 (Na vacancy energy) or two unequal E_2 (substitution energy of Na by Nd) result not only from the displacement of oxygen (as discussed above) but also from the relaxation of Na towards the 18 h position. Still Model I structure shows larger difference between the E_i values.

The E_4 for the non-stoichiometric structure in Table 5 are calculated with Na positioned at 1, 2, 3 in Fig. 10 being replaced by a Nd, which is one of the most stable configurations. Unlike in the stoichiometric β''-alumina, E_4 value is slightly lower than $(E_1 + E_3)$, implying that the next nearest V'_{Na} still has some interaction with the associated defect $V'_{Na}(1)\ldots Nd\ldots V'_{Na}(2)$ and is not independent in the non- stoichiometric β''-alumina.

3.3. Displacement from Ideal Sites

Our result that the eight-coordinated mO site is preferred agrees with the general fact that Nd tend to reside in high coordination sites in oxides. The actual equilibrium site of Nd^{3+} is displaced from the ideal mO position (i.e. X-ray derived) by different amounts, depending on parent crystal structure (stoichiometric or nonstoichiometric), distribution of Mg in the spinel block, and configuration of the nearby Na vacancies. The most probable equilibrium sites of Nd and defect structure should have the lowest defect energy. Since the defect structure caused by Na/Nd substitution

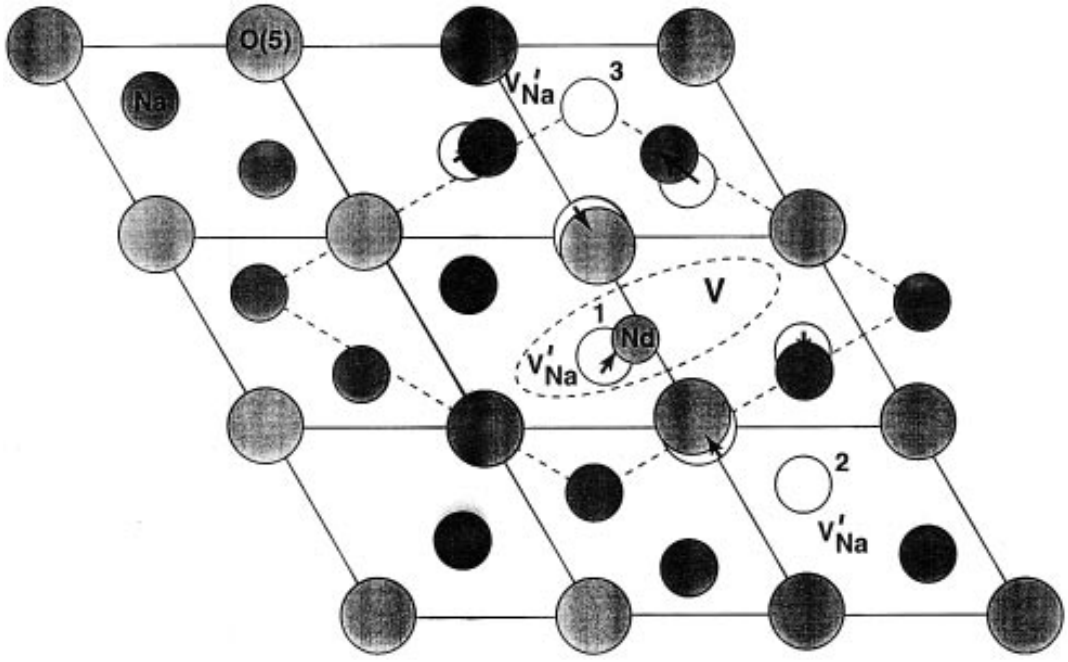

Fig. 10. Structural relaxation upon introduction of one Nd for substitution of three Na^+ positioned at 1, 2, 3 in the non-stoichiometric conduction plane. V is the intrinsic Na vacancy. The defect $V_{Na}(1)\ldots Nd\ldots V_{Na}(2)$ is shown by the dotted oval.

process that give rise to the lowest defect energy always involves the defect $V'_{Na}(1)\ldots Nd\ldots V'_{Na}(2)$, we can use the local structure around $V'_{Na}(1)\ldots Nd\ldots V'_{Na}(2)$ to describe how those atoms Nd, O(3), (4), (5) relax from their ideal position in both the stoichiometric and nonstoichiometric structures. Figures 11 and 12 give the final relaxed local structure for stoichiometric and non-stoichiometric β''-aluminas, respectively. The $V'_{Na}(1)\ldots Nd\ldots V'_{Na}(2)$ defect structure in following discussion is created by the process (3) and (2), respectively, for the stoichiometric and non-stoichiometric β''-aluminas. It should be pointed out that the next nearest V'_{Na}, though is not associated with the $V'_{Na}(1)\ldots Nd\ldots V'_{Na}(2)$, also affects the equilibrium position of Nd and its surrounding oxygen. But such influence is minor, compared with that from the nearest Na vacancy, and thus will not be discussed here.

As indicated in Fig. 8, there is actually no symmetric mO center in either the Model structure. But in the following discussion, we still use the term ''mO site'', which should be referred to the center of four O(4) atoms. In the stoichiometric structure with Model I configuration, Nd^{3+} relaxes off the mO site by about 0.3 Å (Table 6). But with the Model II structure, the displacement from the mO position is calculated as only 0.16 Å, about half of the displacement of the Model I, and is very close to the suggested displacement determined from polarizing absorption spectra by Alfrey et al. [11]. Their model proposed that if the displacement of Nd^{2+} is about 0.2 Å and of O(5) 0.3–0.5 Å, the experimental data can be best fitted [11].

The difference between the Nd^{3+} position in the two β''-aluminas (Models I and II) is evidently due to the different distribution of Mg^{2+} ions in the spinel block. Bush et al. also performed static lattice calculation on Nd^{3+} doped β''-aluminas, using the same approach as this work, but obtained results showing that Nd^{3+} resides midway between mO and BR, the 18 h sites [7]. This position can be

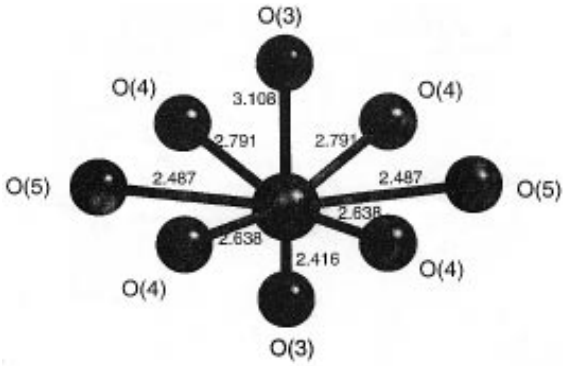

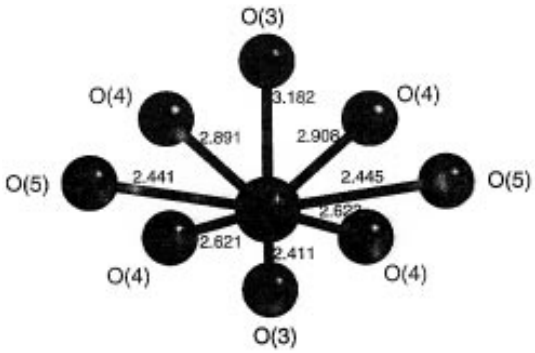

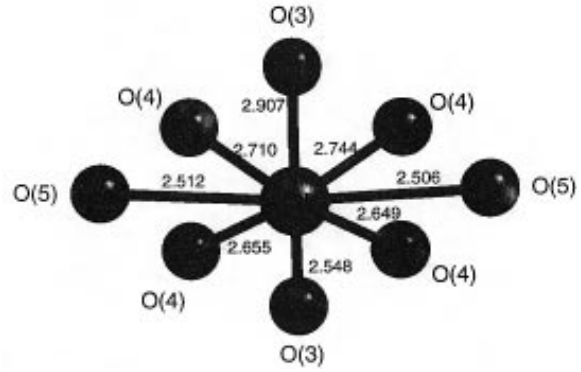

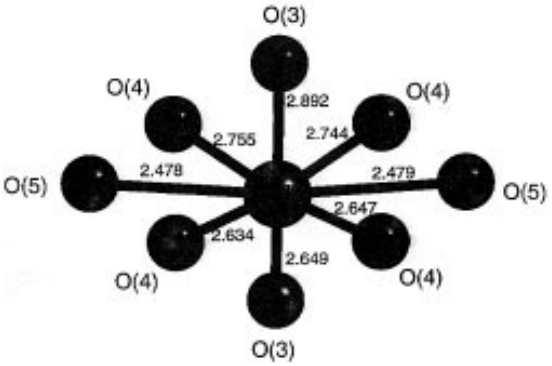

Fig. 11. Local structure around Nd in stoichiometric β''-alumina, (a) Model I, (b) Model II.

Fig. 12. Local structure around Nd in non-stoichiometric β''-alumina, (a) Model I, (b) Model II.

Table 6. Displacement in defect structure $V'_{Na}(1) \ldots Nd \ldots V'_{Na}(2)$ for nearest neighbor in both the stoichiometric and non-stoichiometric β''-alumina

Displacement (Å)				
	$Na_2MgAl_{10}O_{17}$		$Na_{1.66}Mg_{0.66}Al_{10.33}O_{17}$	
energy type	Model I	Model II	Model I	Model II
Nd	0.32	0.16	0.37	0.15
O(5)	0.385	0.390, 0.400	0.377, 0.385	0.386, 0.388
O(4)	0.160, 0.087	0.114, 0.135, 0.149, 0.112	0.176, 0.177, 0.126, 0.142	0.154, 0.170, 0.162, 0.182
O(3)	0.183, 0.077	0.117, 0.180	0.195, 0.116	0.170, 0.158

* The displacement of Nd is from the center of four O(4) atoms.

transformed as a displacement from the ideal mO by ∼0.8 Å , which is too far away from the X-ray derived data and the expectation by Alfrey et al. as well. Although there are no details given in Bush et al.'s report about their potential parameters and input models, we might expect that their inadequate position of Nd is quite possibly caused by unstable Mg configurations in their model.

Another feature of the local structure of Nd^{3+} in the conduction plane is the relaxation of all the nearest oxygen atoms around the Nd^{3+} from their original position (Figs. 11 and 12). The difference between Models I and II is less significant compared with the displacement of Nd itself (Table 6). In both Model structures, the two nearest bridging oxygen ions, O(5), significantly displaced towards Nd by ∼0.39 Å. Such a movement has also been clarified by single crystal X-ray diffraction and EXAFS studies [6,10]. The $Nd^{3+} \ldots O(5)$ distance after relaxation is calculated to be 2.49 and 2.51 Å for Models I and II, respectively, which is close to the value from the X-ray and EXAFS studies (2.46 Å) [6,10]. The nearest oxygen in the spinel block also move towards Nd significantly (Table 7). The trend for the oxygen displacement is almost the same for both Models but more uniformly for Model II. The relaxation of those oxygen can be as much as 0.18 Å, leading to the bond length of one of the Nd . . . O(3) even shorter than Nd . . . O(5) in the Model I structure.

The non-stoichiometric structure showed the same trend of the relaxation around Nd (Tables 6 and 7). Again, the displacement in the Model II structure is more uniform than in Model I. The Nd . . . O(5) bond length is calculated to be 2.44 and 2.48 Å with Model I and II structures (Fig. 12), being closer to the experimental derived values, compared with Models for the stoichiometric structure.

Rocca et al. proposed, on the basis of their EXAFS and XANES spectra analysis, that the shift of the O(5) atoms leads to a relaxation of the four Al(6c) in the opposite direction, so that the Nd-Al(6c) bond length becomes 0.13 Å longer. The six oxygens above and below the conduction plane relax towards Nd by ∼0.1 Å and the shortest bond is between Nd . . . O(5). Our calculation also showed similar movement of Al(6c). The Nd-Al(6) bond length in our model is calculated as 3.20 ∼ 3.35 Å, which is very close to theirs (3.35 Å). The displacement of those oxygens towards Nd in our models is slightly more significant, as shown in Table 6. The shortest Nd-O bond in Model II is also between Nd . . . O(5).

In summary, the above discussion obviously favors

Table 7. Some Nd-O distance (Å) in $Na_2MgAl_{10}O_{17}$ and $Na_{1.66}Mg_{0.66}Al_{10.33}O_{17}$ Interatomic distance (Å)

	X-ray	EXAFS	$Na_2MgAl_{10}O_{17}$		$Na_{1.66}Mg_{0.66}Al_{10.33}O_{17}$	
multiplicity	Ref. 6	Ref. 10	Model I	Model II	Model I	Model II
Nd(2)-O(5) × 2	2.460	2.458	2.487	2.512, 2.506	2.447, 2.441	2.478, 2.479
Nd(2)-O(4) × 2	2.758	2.686	2.791, 2.637	2.655, 2.649, 2.710, 2.744	2.621, 2.623, 2.891, 2.908	2.634, 2.647, 2.744, 2.755
Nd(2)-O(3) × 2	2.781	2.724	3.108, 2.416	2.907, 2.548	2.411, 3.180	2.649, 2.892

the Model II structure, if we consider the better agreement with experimental data. Even the less stable, however, Model I structure may also be possible, since Mg distribution in β''-aluminas is variable and also depends on the condition of sample preparation. From neutron diffraction study, Alden et al. found that the quenching rate, which showed influence upon the electrical conductivity, affects upon the Mg distribution, i.e., faster quenching rate leads to more randomness of Mg distribution [21]. If the Mg distribution is frozen to some relatively unstable configuration, like in Model I structure, by well controlling the rapid quenching rate or other method, Nd^{3+} ions, which are exchanged for Na^+ at low temperature should be displaced more than 0.16 Å from mO site. In other words, the local structure of Nd in β''-aluminas, which dominate the optical properties of Nd^{3+}, can vary significanly, not only depending on the stoichiometry but also on the sample preparation condition.

4. Conclusions

We have studied the structure of Nd^{3+} doped β''-aluminas through atomistic computer simulation and reached following conclusions:

1. Nd^{3+} ions are preferentially located in distorted mO positions with two next nearest Na sites (BR) being vacant. The Model II structure, in which the Mg ions tend to aggregate as two- or three-membered clusters and to form a 2D triple superlattice, is mostly favored. The displacement of Nd from the ideal mO site is $\sim$0.16 Å. This value is subject to minor change, depending on the actual location of next nearest Na^+ vacancies.
2. The nearest mid-oxygen in the conduction plane are displaced towards the Nd^{3+} by $\sim$0.39 Å, which agrees well with experimental studies. Other oxygen in the spinel block which are adjacent to Nd^{3+}, but are less mobile, also relax towards Nd^{3+} non-uniformly, leading to a narrowing of the conduction slab. The two nearest Al(6c) ions in the spinel block are repelled in opposite directions.
3. The displacement of both Nd^{3+} and its surrounding oxygen ions from their original positions breaks the inversion symmetry at the ideal mO site, which allows the strong optical absorption of Nd^{3+} in β''-aluminas to be seen experimentally. Both the presence of Mg and V'_{Na} contribute to this. Our calculation suggests that the local structure of Nd^{3+} and therefore, the optical properties of Nd doped β''-aluminas can be changed by controlling sample preparation conditions, such as quenching rate.

Acknowledgments

We are grateful to the U.S. Department of Energy, Office of Basic Energy Sciences for financial support under grant number DE-FG02-91ER45451. Some of the calculations reported here were performed at the Cornell Theory Center, which is funded in part by New York State, the National Science Foundation and IBM corporation.

References

1. M. Jansen, A.J. Alfrey, O.M. Stafsudd, B. Dunn, D.L. Yang, and G.C. Farrington, *Opt. Lett*., **9**, 119 (1984).
2. R.W. Boyd, M.T. Gruneisen, P. Narum, D.J. Simkin, B. Dunn, and D.L. Yang, *Opt. Lett*., **11**, 11 (1986).
3. M. Laberge, D.J. Simkin, and B. Duun, *J. Chem. Phys*., **96**, 5565 (1992).
4. B. Dunn and G.C. Farrington, *Solid State Ionics* **9/10**, 223 (1983).
5. P. Davies, A. Petford and M. ÓKeefe, *Solid State Ionics* **18/19**, 624 (1986).
6. W. Carrillo-Cabrera, J.O. Thomas, and G.F. Farrington, *Solid State Ionics* **28–30**, 317 (1988).
7. T.S. Bush, C.R. A. Catlow, A.V. Chadwick, M.Cole, R.M. Geatches, G.N. Greaves, and S.M. Tomlinson, *J. Mater. Chem*., **2**, 309 (1992).
8. M. Wolf and J.O. Thomas, *Acta Cryst*., **B49**, 491 (1993).
9. M. Wolf, Sedvardsson, M.A. Zendejas, and J.O. Thomas, *Phys. Rev*., **B48**, 10129 (1993).
10. F. Rocca, A. Kuzmin, J. Purans, and G. Mariotto, *Phys, Rev*., **B50**, 6662 (1994).
11. A.J. Alfrey, O.M. Stafsudd, B. Dunn, and D.L. Yang, *J. Chem. Phys*., **88**, 707 (1988).
12. J.G. Park and A.N. Cormack, *J. Solid State Chem*., **121**, 278 (1996).
13. J.G. Park and A.N. Cormack, *Philos. Mag*., **B73**, 21 (1996).
14. A.N. Cormack, *Solid State Ionics*, **8**, 187 (1983).
15. G.V. Lewis and C.R.A. Catlow, *J. Phys*., **C18**, 1149 (1985).
16. C.R.A. Catlow, *Proc. R. Soc*., London **A353**, 533 (1977).
17. M.Bettman and C.R. Peters, *J. Phys. Chem*., **73**, 1774 (1969).
18. W.L. Roth, F. Reidinger and S. La Placa, in *Superionic Conductor*, edited by G.D. Mahan and W.L. Roth (Plenum, New York, 1976), p. 223.
19. J.B. Bates, A.M. Brown, T.Kaneda, W.E. Brundage, J.C. Wang, and H. Engstrom, in *Fast Ionic Transport in Solids*, edited by P. Vashishta, J.N. Mundy and G.K. Shenoy (North-Holland, New York, 1979), p. 261.
20. J.O. Thomas and G.C. Farrington, *Acta Cryst*., **B39**, 227 (1983).

21. M. Alden, J.O. Thomas, and P. Davies, *Solid State Ionics*, **18/19**, 694 (1986).
22. B. Hafskjold and X. Li, *J. Phys.: Condens. Matter*, **7**, 2949 (1995).
23. J.P. Boilot, G. Collin, Ph. Colomban, and R. Comes, *Phys. Rev.*, **B22**, 5912 (1980).
24. M.L. Wolf, J.R. Walker, and C.R.A. Catlow, *Solid State Ionics*, **13**, 33 (1984).